Rayleigh Wave Propagation in an Anisotropic Half-Space with a Graded Piezoelectric Capping Layer and a Non-Ideal Interface

Abdulkhamid Kholmurodov
Department of Applied Mathematics, Karshi State University, Karshi, Uzbekistan
abishx@mail.ru

Muhammad Matanov
Department of Applied Mathematics, Karshi State University, Karshi, Uzbekistan
mm939011166@gmail.com (corresponding author)

Received: 15 October 2025 | Revised: 11 January 2026 and 19 January 2026 | Accepted: 31 January 2026

 DOI: https://doi.org/10.48084/etasr.15548

ABSTRACT

This study examines Rayleigh-wave propagation in an anisotropic piezoelectric half-space coated with a functionally graded piezoelectric capping layer, accounting for a non-ideal interfacial condition. The state-space transport equation is first derived from the governing field equations and constitutive relations. The resulting system is then solved to obtain the state-vector transfer matrix and the associated stiffness matrix. An overall surface stiffness matrix is constructed by assembling the contributions of the piezoelectric substrate, the graded capping layer, and the non-ideal interface through appropriate matrix coupling. The frequency–dispersion relation is subsequently formulated by imposing electrically open-circuit and short-circuit conditions, together with a mechanically traction-free boundary condition at the surface. Five graded capping-layer profiles are investigated, in which material properties vary smoothly through the thickness, along with two non-ideal interface models: (i) a dielectric, weakly conducting interface and (ii) a highly conducting yet mechanically compliant interface. Numerical results demonstrate that the Rayleigh-wave phase velocity is strongly influenced by the selected gradient profile, particularly when both mechanical and dielectric interfacial non-idealities are present.

Keywords-gradient capping layer; non-ideal interface; piezoelectricity; state transfer equation; surface stiffness matrix; surface wave

I. INTRODUCTION

The study of Surface Acoustic Waves (SAWs) in inhomogeneous media constitutes a key research direction in materials science and acoustic device engineering, owing to its direct relevance to wave control and device miniaturization. In particular, functionally graded piezoelectric layers and non-ideal interfacial conditions have attracted sustained attention, as they can substantially modify dispersion characteristics and thereby enable performance improvements in modern sensors, high-frequency filtering components, and Micro-Electromechanical Systems (MEMS).

SAWs underpin the operation of a wide range of devices, including telecommunication filters, ultrasonic sensors, and control-system components. The seminal study by authors in [1] on SAW propagation in media with spatially varying parameters established that material inhomogeneity can markedly modify dispersion characteristics—an effect that must be accounted for in acoustic-device design. Authors in [2] provided a comprehensive treatment of acoustic waves in periodic structures, emphasizing their practical significance for signal filtering and acousto-optic applications. Authors in [3] presented an in-depth analysis of SAW technologies for telecommunications, documenting major advances in signal-processing architectures based on piezoelectric substrates.

Rayleigh-wave propagation in gradient elastic structures was examined in a foundational manner by authors in [4]. The investigations by authors in [5] on thermoelastic Rayleigh waves in exponentially graded half-spaces are particularly pertinent to temperature-sensitive sensing applications. Authors in [6] further demonstrated that damage in piezoelectric materials can substantially influence Rayleigh-wave characteristics; this line of inquiry was extended by authors in [7], who analyzed dislocation–interface interactions in piezoelectric laminates and their implications for wave propagation.

The role of non-ideal interfaces in shaping wave characteristics is increasingly recognized as a key factor in improving the accuracy and precision of acoustic devices. Authors in [8] demonstrated that functionally graded piezoelectric materials can exhibit pronounced sensitivity to

interfacial parameters, and systematically quantified the effects of mechanically compliant and dielectrically imperfect interfaces on Rayleigh-wave dispersion. Beyond classical piezoelectric configurations, recent progress in modeling wave propagation in complex media—such as nonlocal orthotropic thermoelastic–diffusive materials with porosity [9, 10]—further emphasizes the necessity of incorporating both gradient effects and refined interface descriptions to obtain reliable dispersion predictions and device-level performance estimates. From a broader theoretical perspective, continuum-based formulations for coupled mechanical and transport processes have been developed extensively within filtration theory and the theory of multiphase media. In particular, the continuum framework proposed by authors in [11] provides a rigorous mathematical foundation for coupled field equations in heterogeneous materials with internal transport mechanisms; this formulation has been adopted widely in advanced studies of wave propagation and porous media, where the interplay between mechanical fields, transport phenomena, and interfacial conditions is essential.

This work provides a comprehensive analysis of Rayleigh-wave propagation in a layered configuration consisting of an anisotropic half-space, a functionally graded piezoelectric capping layer, and a non-ideal interface. The principal contributions are as follows: (i) a unified state-space transfer-matrix formulation that captures, in a coupled manner, the combined influence of material grading and interfacial non-idealities; (ii) an efficient computational strategy for functionally graded layers based on high-order Magnus expansions supplemented by Padé approximants; and (iii) a systematic parametric study of five representative gradient profiles and two non-ideal interface models, yielding quantitative guidance for the design, optimization, and diagnostics of advanced SAW devices.

In a broader computational context, numerical techniques for wave propagation in elastic continua have progressed toward improved stability and accuracy under dynamic loading. In particular, hybrid and semi-analytical approaches have been shown to provide reliable predictions of surface- and body-wave responses in half-space settings under complex boundary conditions and transient excitations [12].

Recent advances in the theory of wave propagation in complex continua include investigations of thermoelastic diffusion in nonlocal orthotropic porous media and analyses of Rayleigh-type waves in nonlocal orthotropic thermoelastic media with diffusion [13, 14]. The former study establishes an analytical framework for assessing the coupled influence of nonlocal elasticity, porosity, and mass diffusion on the resulting material response. The latter examines dispersion and attenuation of Rayleigh-type surface waves under thermoelastic–diffusive coupling in a nonlocal orthotropic setting, thereby clarifying the extent to which interacting physical mechanisms may govern surface-wave characteristics in advanced materials. Collectively, these contributions reflect growing interest in incorporating nonlocality and diffusion into surface-wave modeling and motivate the development of more comprehensive formulations for related layered and interfacial configurations.

The novelty of this study lies in the development of a unified analytical–numerical framework for Rayleigh-wave propagation that simultaneously incorporates continuous material grading within a piezoelectric capping layer, mechanically and dielectrically non-ideal interfacial conditions, and anisotropy of the underlying substrate. In contrast to prior studies that typically address these effects in isolation or approximate graded layers through layer-wise discretization, the present work employs a state-space transfer-matrix formulation solved using a high-order Magnus expansion combined with Padé approximation. This approach provides a stable and accurate treatment of continuously graded media and enables systematic quantification of the coupled effects of gradient profiles, interfacial imperfections, and electrical boundary conditions on surface-wave dispersion.

II. THEORETICAL FORMULATION

A. *Stiffness Matrix of the Gradient Capping Layer*

Consider an anisotropic elastic homogeneous half-space coated with a gradient piezoelectric layer, separated by a non-ideal interface, as depicted in Figure 1.

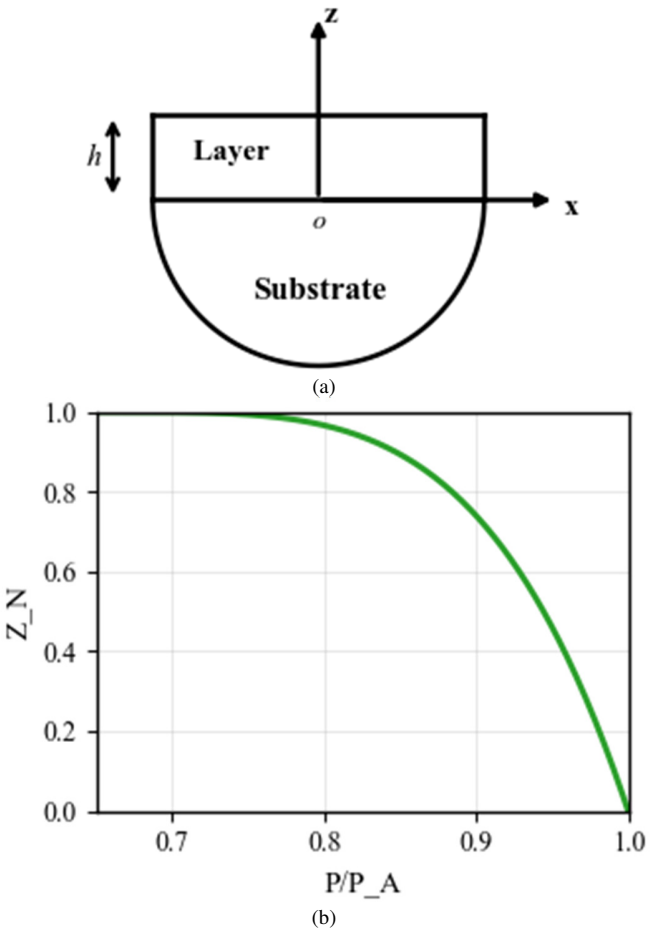

Fig. 1. Homogeneous elastic half-space with a graded piezoelectric capping layer: (a) geometry of the half-space and layer, (b) exemplary profiles of material parameter variation within the capping layer.

The dispersion relation for Rayleigh surface waves is obtained by first evaluating the stiffness matrices associated with the capping layer and the substrate, and subsequently combining them to form the overall surface stiffness matrix for the layered configuration. The governing equations together with the constitutive relations of a linear piezoelectric solid can be written, following [15], as:

$$\sigma_{ij,j} = \rho \ddot{u}_i, \quad D_{i,i} = 0 \tag{1}$$

$$\sigma_{ij} = c_{ijkl} u_{k,l} + e_{kij} \phi_{,k}, \quad D_i = e_{ikl} u_{k,l} - \epsilon_{ik} \phi_{,k} \tag{2}$$

where σ_{ij} is the stress tensor, u_i is the mechanical displacement vector, ϕ is the electric potential, D_i is the electrical displacement vector, c_{ijkl}, e_{kij}, and ϵ_{ik} are the elastic, piezoelectric, and dielectric constants, respectively, and ρ is the mass density. For wave motion, the solution is sought in the form:

$$\{u_i, \phi\}^T = \left\{\hat{u}_i(z), \hat{\phi}(z)\right\}^T e^{ik(x-vt)} \tag{3}$$

where k is the wavenumber and v is the phase velocity. Defining a state vector $\eta(z) = \left[\hat{u}_x, \hat{u}_z, \hat{\phi}, \hat{\sigma}_{zz}, \hat{\sigma}_{xz}, \hat{D}_z\right]^T$, the governing equations reduce to a first-order matrix differential equation for the inhomogeneous layer [16]:

$$\frac{d\eta(z)}{dz} = \mathrm{A}(z)\eta(z) \tag{4}$$

Here, $\mathrm{A}(z)$ is a 6 × 6 matrix whose elements depend on the material properties, wavenumber k, frequency ω, and the gradient profiles. Equation (4) is the state transfer equation. A transfer matrix $\mathrm{T}(z, z_0)$ relates state vectors at two depths:

$$\eta(z) = \mathrm{T}(z, z_0)\eta(z_0) \tag{5}$$

$$\frac{d\mathrm{T}(z, z_0)}{dz} = \mathrm{A}(z)\mathrm{T}(z, z_0), \quad \mathrm{T}(z, z_0) = \mathrm{I} \tag{6}$$

The solution to (6) can be formally written as:

$$\mathrm{T}(z, z_0) = \exp\left(\int_{z_0}^{z} \mathrm{A}(\xi)\, d\xi\right) \tag{7}$$

For a layer with properties varying with z, the direct computation of (7) is difficult. We employ the Magnus expansion [9, 10]:

$$\mathrm{T}(z_0 + h, z_0) = \exp(\Omega(h)) \tag{8}$$

$$\Omega(h) = \sum_{k=1}^{\infty} \Omega_k(h) \tag{9}$$

where $\Omega_k(h)$ are integrals involving commutators of $\mathrm{A}(z)$. The moments matrices are defined as [17]:

$$\begin{aligned} \mathrm{A}_1 &= \frac{1}{h}\int_{z_0}^{z_0+h} \mathrm{A}(\xi)\, d\xi, \\ \mathrm{A}_2 &= \frac{12}{h^3}\int_{z_0}^{z_0+h} (\xi - z_0 - h/2)\mathrm{A}(\xi)\, d\xi, \end{aligned} \tag{10}$$

A sixth-order truncated Magnus series is used:

$$\Omega(h) \approx h\mathrm{A}_1 + \frac{h^3}{12}(-\mathrm{A}_1\mathrm{A}_2 + \mathrm{A}_2\mathrm{A}_1) + \ldots \tag{11}$$

The matrix exponential in (8) is then evaluated using an eighth-order diagonal Padé approximation. The surface stiffness matrix K of the layer, defined by the relation between generalized tractions t and displacements u at its surface $(z = 0)$, is obtained from the transfer matrix:

$$\mathrm{t}(0) = \mathrm{K}_u(0) \tag{12}$$

B. Stiffness Matrix of a Homogeneous Piezoelectric Half-Space

For a homogeneous half-space $(z > H)$, the matrix A in (4) is constant. Let λ_m and ξ_m $(m = 1, \ldots, 6)$ be the eigenvalues and eigenvectors of A. They are partitioned into two sets: λ_p with $\mathrm{Re}(\lambda_p) < 0$ or $\mathrm{Im}(\lambda_p) > 0$, and λ_q with $\mathrm{Re}(\lambda_q) > 0$ or $\mathrm{Im}(\lambda_q) < 0$, corresponding to waves decaying as $z \to +\infty$ and $z \to -\infty$, respectively. The matrix of eigenvectors is partitioned as:

$$\Xi = \begin{bmatrix} \Xi_u \\ \Xi_t \end{bmatrix} = \begin{bmatrix} \Xi_{u_1} & \Xi_{u_2} \\ \Xi_{t_1} & \Xi_{t_2} \end{bmatrix} \tag{13}$$

and its inverse as:

$$\Xi^{-1} = \begin{bmatrix} \Xi^1 & \Xi^2 \end{bmatrix} = \begin{bmatrix} \Xi_u^1 & \Xi_t^1 \\ \Xi_u^2 & \Xi_t^2 \end{bmatrix} \tag{14}$$

For a substrate occupying $z > H$, only the three eigenvalues with negative real parts (denoted $\lambda_j^{(s)}$, $j = 1, 2, 3$) are physically admissible. The transfer matrix for the substrate is:

$$\mathrm{T}_s = \begin{bmatrix} \mathrm{U}_{s_1} \\ \mathrm{U}_{s_2} \end{bmatrix} = \begin{bmatrix} \Xi_u^{(s)} \\ \Xi_t^{(s)} \end{bmatrix} \Lambda_s(z - H) \tag{15}$$

where $\Xi_u^{(s)}$ and $\Xi_t^{(s)}$ contain the displacement and traction components of the relevant eigenvectors, and $\Lambda_s(z) = \mathrm{diag}[e^{\lambda_1^{(s)} z}, e^{\lambda_2^{(s)} z}, e^{\lambda_3^{(s)} z}]$. The relation at the interface $z = H$ is:

$$\eta(H) = \begin{bmatrix} \mathrm{u}(H) \\ \mathrm{t}(H) \end{bmatrix} = \begin{bmatrix} \Xi_u^{(s)}\Lambda_s(0) \\ \Xi_t^{(s)}\Lambda_s(0) \end{bmatrix} \mathrm{c} = \begin{bmatrix} \Xi_u^{(s)} \\ \Xi_t^{(s)} \end{bmatrix} \mathrm{c} \tag{16}$$

where c is a constant vector. Eliminating c gives the surface stiffness matrix of the half-space K_s:

$$\mathrm{K}_s = \Xi_t(s)\left(\Xi_u^{(s)}\right)^{-1} \tag{17}$$

C. Stiffness Matrix for a Non-Ideal Interface

Under ideal bonding, the displacement field, traction vector, electric potential, and normal electric displacement are continuous across the interface. Real interfaces may deviate from this idealization due to imperfect bonding, thin interphases, or microstructural defects. Consistent with [18, 19], we represent these effects using a zero-thickness interface model with linear interfacial constitutive laws, in which discontinuities in displacement and electric potential are related linearly to the interfacial traction and normal electric displacement, respectively.

1. Mechanically Compliant and Dielectrically Weakly Conducting Interface:

$$[\![\mathrm{u}]\!] = \mathrm{R}_m \mathrm{t}^{(1)}, [\![\phi]\!] = R_d D_z^{(1)} \tag{18}$$

where $[\![\cdot]\!]$ denotes the jump across the interface, superscripts (1) and (2) denote substrate and layer sides, $\mathrm{R}_m = \mathrm{diag}[R_{m1}, R_{m2}]$ and R_d are interface compliance parameters. The limiting cases $R_{m1}, R_{m2}, R_d \to 0$ represent an ideal interface, whereas $R_{mi} \to \infty$ signifies complete mechanical debonding, and $R_d \to \infty$ represents a perfectly insulating interface. The transfer matrix $\mathrm{T}_{int}^{(1)}$ for this interface type can be expressed as:

$$\mathrm{T}_{int}^{(1)} = \begin{bmatrix} \mathrm{I} & 0 \\ \mathrm{R}_m^{-1} & \mathrm{I} \end{bmatrix} \tag{19}$$

$$\mathrm{K}_{int}^{(1)} = \begin{bmatrix} \mathrm{R}_m^{-1} & -\mathrm{I} \\ \mathrm{I} & 0 \end{bmatrix} \tag{20}$$

2. Mechanically Compliant and Dielectrically Highly Conducting Interface:

$$[\![\mathrm{u}]\!] = \mathrm{R}_m \mathrm{t}^{(1)}, \; D_z^{(1)} = D_z^{(2)} = 0 \tag{21}$$

This model assumes perfect electrical contact (continuous ϕ) but allows mechanical slip. The corresponding transfer relation is:

$$\mathrm{T}_{int}^{(2)} = \begin{bmatrix} \mathrm{I} & 0 \\ \mathrm{R}_m^{-1} & \mathrm{I} \end{bmatrix} \tag{22}$$

D. Overall Surface Stiffness Matrix and Dispersion Relation

For two layers with ideal interface, if their transfer and stiffness matrices are known:

$$\mathrm{T}^{(1)}, \mathrm{K}^{(1)}; \quad \mathrm{T}^{(2)}, \mathrm{K}^{(2)} \tag{23}$$

then the combined transfer and stiffness matrices are:

$$\begin{aligned} &\mathrm{T} = \mathrm{T}^{(2)}\mathrm{T}^{(1)}, \\ &\mathrm{K} = \mathrm{K}^{(2)} + \mathrm{T}^{(2)}\mathrm{K}^{(1)}\left(\mathrm{I} - \mathrm{S}^{(2)}\mathrm{K}^{(1)}\right)^{-1}\mathrm{T}^{(2)T} \end{aligned} \tag{24}$$

where $\mathrm{S}^{(2)}$ is derived from $\mathrm{T}^{(2)}$. For the capping layer with a non-ideal interface (Type 1), the equivalent transfer matrix and stiffness matrix are:

$$\begin{aligned} &\mathrm{T}_{eq} = \mathrm{T}_{cap}\mathrm{T}_{int}^{(1)}, \\ &\mathrm{K}_{eq} = \mathrm{K}_{cap} + \mathrm{T}_{cap}\mathrm{K}_{int}^{(1)}\left(\mathrm{I} - \mathrm{S}_{cap}\mathrm{K}_{int}^{(1)}\right)^{-1}\mathrm{T}_{cap}^{T} \end{aligned} \tag{25}$$

Then the overall transfer matrix and stiffness matrix for the half-space with capping layer and non-ideal interface are:

$$\begin{aligned} &\mathrm{T}_{total} = \mathrm{T}_s\mathrm{T}_{eq}, \\ &\mathrm{K}_{total} = \mathrm{K}_s + \mathrm{T}_s\mathrm{K}_{eq}(\mathrm{I} - \mathrm{S}_s\mathrm{K}_{eq})^{-1}\mathrm{T}_s^{T} \end{aligned} \tag{26}$$

The overall surface stiffness matrix relates the generalized traction vector $\mathrm{t}(0)$ to the generalized displacement vector $\mathrm{u}(0)$ at the surface:

$$\mathrm{t}(0) = \mathrm{K}_{total}\mathrm{u}(0) \tag{27}$$

The dispersion relation is obtained by imposing mechanical and electrical boundary conditions at the top surface $(z = 0)$.

1. Electrically open-circuit and mechanically stress-free surface:

$$\sigma_{xz}(0) = \sigma_{zz}(0) = 0, \quad D_z(0) = 0 \tag{28}$$

Substituting into (27) leads to a homogeneous system. The existence of a non-trivial solution requires:

$$\det\left(\begin{bmatrix} K_{41} & K_{42} & K_{43} \\ K_{51} & K_{52} & K_{53} \\ K_{61} & K_{62} & K_{63} \end{bmatrix}\right) = 0 \tag{29}$$

where K_{ij} are elements of K_{total}. Equation (29) is the dispersion relation for this case.

2. Electrically short-circuit and mechanically stress-free surface:

$$\sigma_{xz}(0) = \sigma_{zz}(0) = 0, \quad \phi(0) = 0 \tag{30}$$

Substituting into (27) gives:

$$\begin{bmatrix} K_{41} & K_{42} & K_{43} \\ K_{51} & K_{52} & K_{53} \\ K_{61} & K_{62} & K_{63} \end{bmatrix}\begin{bmatrix} u_x(0) \\ u_z(0) \\ \phi(0) \end{bmatrix} = 0 \tag{31}$$

With $\phi(0) = 0$, a non-trivial solution exists when:

$$\det\left(\begin{bmatrix} K_{41} & K_{42} \\ K_{51} & K_{52} \end{bmatrix}\right) = 0 \tag{32}$$

where $K_{ij}^{*} = K_{ij} - K_{i3}K_{3j} / K_{33}$ (for $i, j = 1, 2$). Equation (32) is the dispersion relation for the short-circuit case.

E. Material Gradient Profiles

The material properties in the graded capping layer vary according to:

$$\mathrm{P}(z) = \mathrm{P}^{(b)} + (\mathrm{P}^{(t)} - \mathrm{P}^{(b)}) f(z / H) \tag{33}$$

where $\mathrm{P}^{(b)}$ and $\mathrm{P}^{(t)}$ are properties at bottom and top, and $f(\zeta)$ is a profile function. We investigate five profiles:

$$\begin{aligned} &\text{Case } 1: f(\zeta) = \zeta; \\ &\text{Case } 2: f(\zeta) = \zeta^2; \\ &\text{Case } 3: f(\zeta) = \zeta; \\ &\text{Case } 4: f(\zeta) = sin(\pi\zeta / 2); \\ &\text{Case } 5: f(\zeta) = 1 - cos(\pi\zeta / 2) \end{aligned} \tag{34}$$

III. NUMERICAL RESULTS AND DISCUSSION

We consider an isotropic elastic substrate coated with a graded, transversely isotropic piezoelectric layer (PZT-5H) of thickness H , with a non-ideal interface between them, as shown in Figure 1. The substrate material constants (λ, μ, ρ_s) are given in Table I. The material properties at the bottom $(z = H)$ and top $(z = 0)$ of the capping layer are denoted as $\mathrm{P}^{(b)}$ and $\mathrm{P}^{(t)}$, respectively, with $\mathrm{P}^{(b)}$ corresponding to standard PZT-5H parameters (Table II). The property variation through the layer thickness follows the power-law profile of (33).

TABLE I. SUBSTRATE (ISOTROPIC ELASTIC) MATERIAL CONSTANTS

Parameter	$\boldsymbol{\lambda}$ **(GPa)**	$\boldsymbol{\mu}$ **(GPa)**	$\boldsymbol{\rho_s}$ **(kg/m^3)**
Value	78.5	16.1	2,200

TABLE II. MATERIAL CONSTANTS FOR PZT-5H AT THE BOTTOM OF THE CAPPING LAYER $(z = H)$ [9, 20]

Elastic $\boldsymbol{c_{ij}}$ **(GPa)**	**Piezoelectric** $\boldsymbol{e_{ij}}$ **(C/m^2)**	**Dielectric** $\boldsymbol{\epsilon_{ij}}$ **(nF/m)**	**Density** $\boldsymbol{\rho_c}$ **(kg/m^3)**
$c_{11} = 151,$ $c_{12} = 98,$ $c_{13} = 96,$ $c_{33} = 124,$ $c_{44} = 23$	$e_{31} = -5.1,$ $e_{33} = 27,$ $e_{15} = 17$	$\epsilon_{11} = 15,$ $\epsilon_{33} = 13.27$	7,500

A. Effects of the Gradient Capping Layer

Figure 2 illustrates the five gradient profiles for two scenarios: (a) $\mathrm{P}^{(t)} > \mathrm{P}^{(b)}$ and (b) $\mathrm{P}^{(t)} < \mathrm{P}^{(b)}$. Figures 3 and 4 show the corresponding dispersion curves for an ideal interface. The wave velocity is sensitive to the gradient profile. For $\mathrm{P}^{(t)} > \mathrm{P}^{(b)}$, the velocity for Case 3 is higher than for Case 1 at low frequencies ($kH < 1$), reversing at higher frequencies. Cases 4 and 5 show similar velocities at low frequencies but diverge at high frequencies. The influence of the surface electrical condition is significant: the effects of different gradient profiles are more pronounced under short-circuit conditions (Figure 3(b)) than under open-circuit conditions (Figure 3(a)). For $\mathrm{P}^{(t)} < \mathrm{P}^{(b)}$ (Figure 4), the behavior is different: Case 3 gives lower velocity than Case 1 at low frequencies, again reversing at high frequencies. In this scenario, the dispersion curves are nearly insensitive to the surface electrical condition.

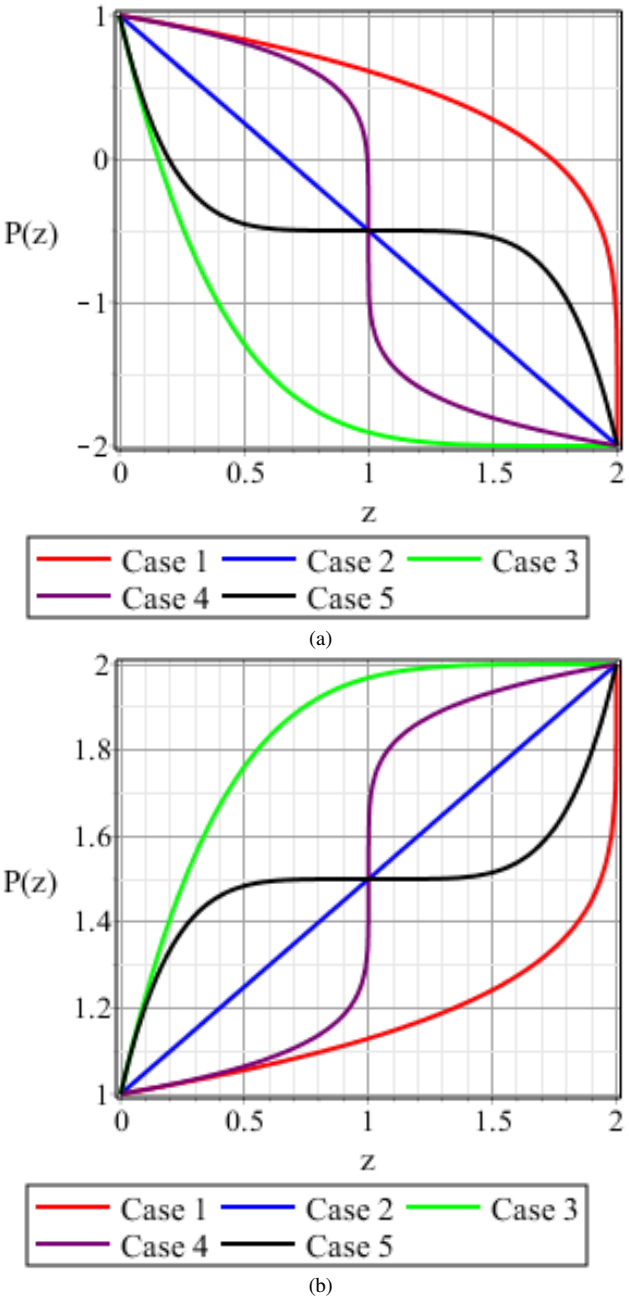

Fig. 2. Five types of gradient profiles for the capping layer, showing the variation of a representative material parameter: (a) $\mathrm{P}^{(t)} > \mathrm{P}^{(b)}$, (b) $\mathrm{P}^{(t)} < \mathrm{P}^{(b)}$.

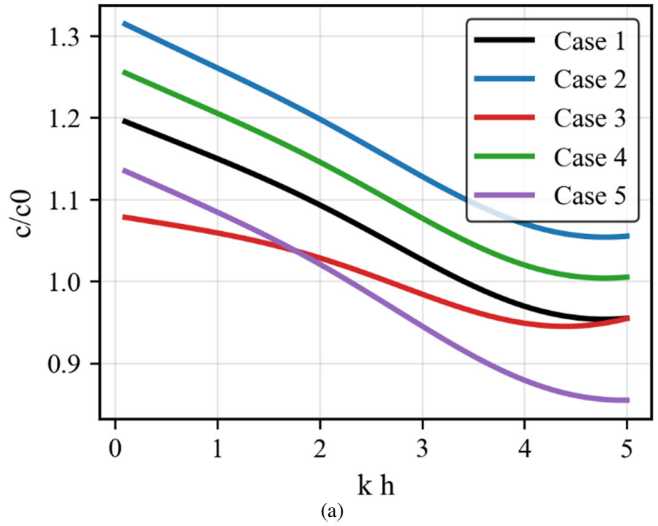

(a)

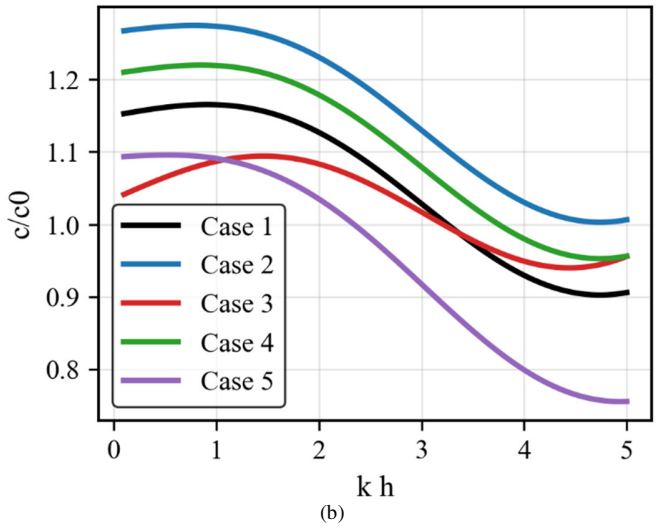

(b)

Fig. 3. Effect of five gradient profiles on dispersion curves in the case of an ideal interface and $P^{(t)} > P^{(b)}$: (a) open circuit, (b) short circuit.

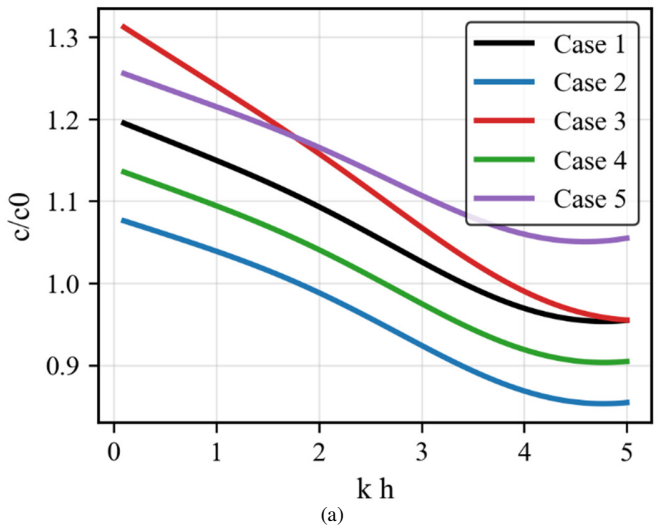

(a)

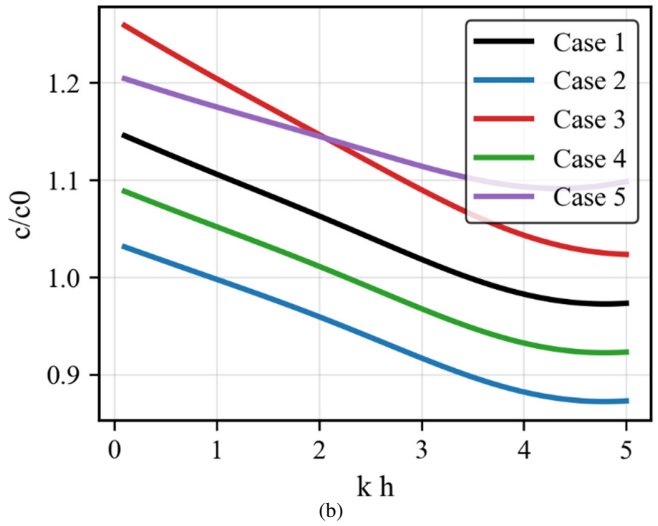

(b)

Fig. 4. Effect of five gradient profiles on dispersion curves in the case of an ideal interface and $P^{(t)} < P^{(b)}$: (a) open circuit, (b) short circuit.

Figure 5 shows the dispersion curve for a homogeneous capping layer for comparison. It exhibits a monotonic decrease in velocity with increasing kH, asymptotically approaching a constant value. The graded layers produce distinctly non-monotonic and profile-dependent behaviors, especially at higher frequencies. This demonstrates that tailored gradient profiles offer a powerful means to control SAW dispersion for specific device applications.

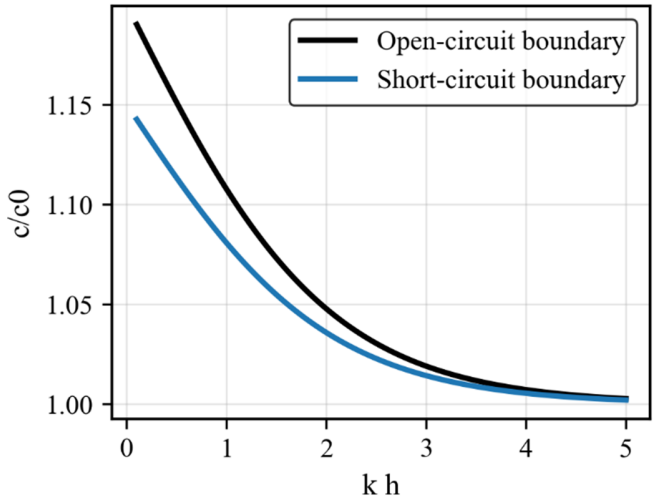

Fig. 5. Dispersion curves for a homogeneous capping layer with an ideal interface.

B. Effects of a Non-Ideal Interface

We now consider two non-ideal interface types with a fixed gradient profile (Case 1, $P^{(t)} > P^{(b)}$). The mechanical non-ideality is governed by parameters $R_{m1} = R_{m2} = R_m$, and the dielectric non-ideality by R_d (for Type 1) or the condition $D_z = 0$ (for Type 2).

Figures 6 and 7 show the effect of the mechanical compliance parameter R_m on wave velocity for a Type 1 (weakly conducting) interface. As R_m increases (i.e., as the interface becomes more compliant), the Rayleigh wave velocity decreases under both open and short-circuit conditions. This behavior is physically consistent, as a softer interface reduces the effective stiffness of the composite structure. The sensitivity to R_m is highest in the low-to-mid frequency range $(\mathrm{kH} < 2)$.

The influence of the dielectric parameter R_d for the Type 1 interface is shown in Figure 8. A larger R_d (more insulating interface) also leads to a reduction in wave velocity, though the effect is generally less pronounced than that of mechanical compliance. This is attributed to the altered electromechanical coupling across the interface.

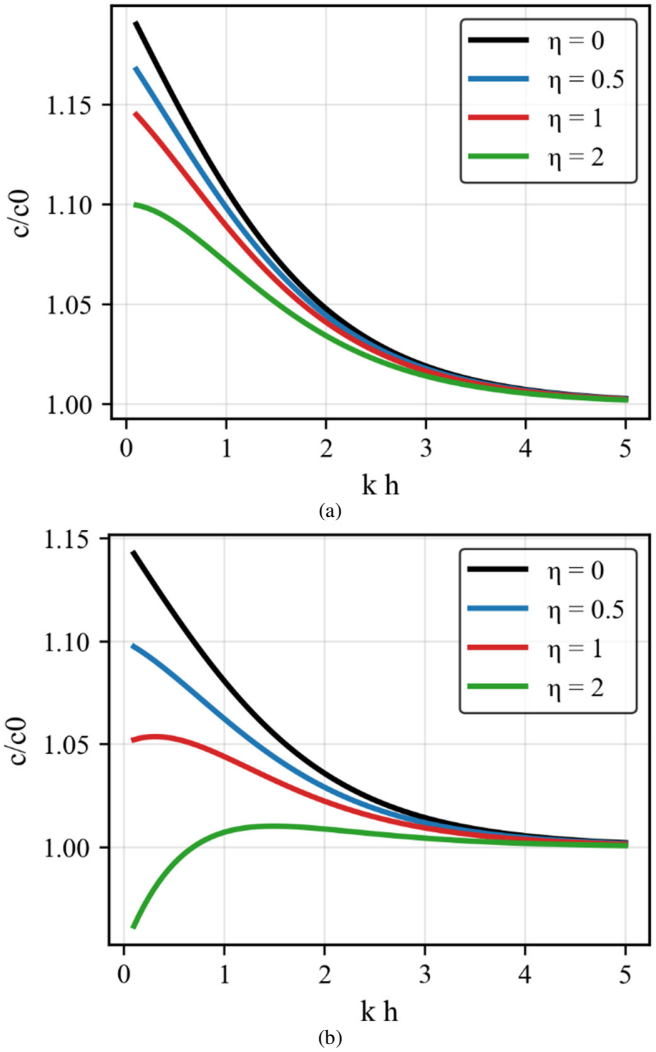

Fig. 6. Effect of interface parameter R_m on surface wave velocity at a dielectric weakly conducting interface (Type 1): (a) open circuit, (b) short circuit.

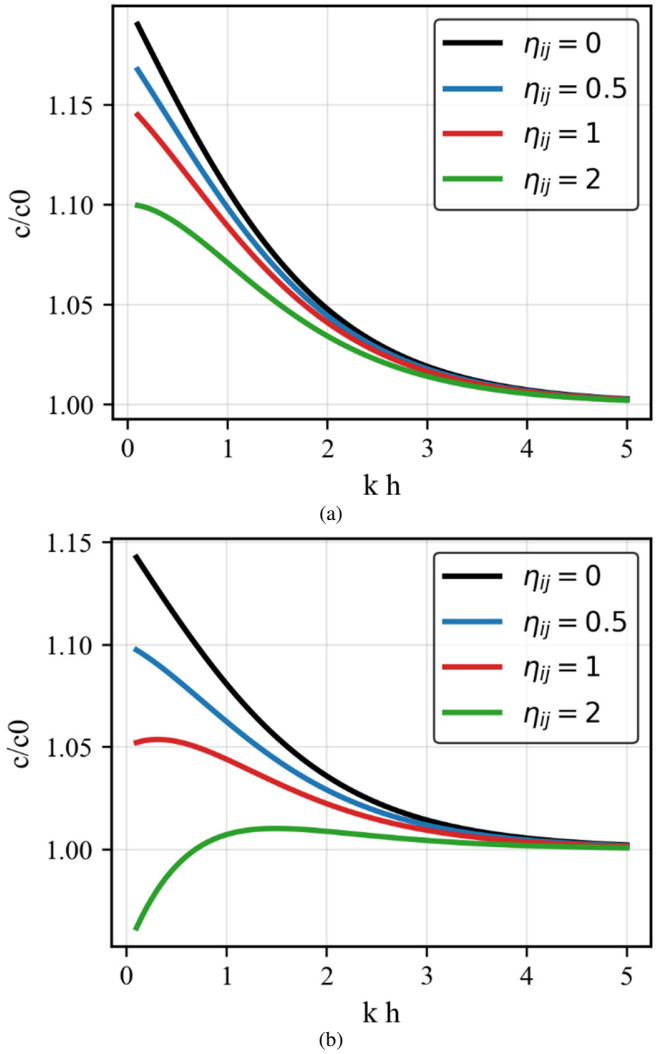

Fig. 7. Effect of interface parameter R_d on surface wave velocity at a dielectric weakly conducting interface (Type 1): (a) open circuit, (b) short circuit.

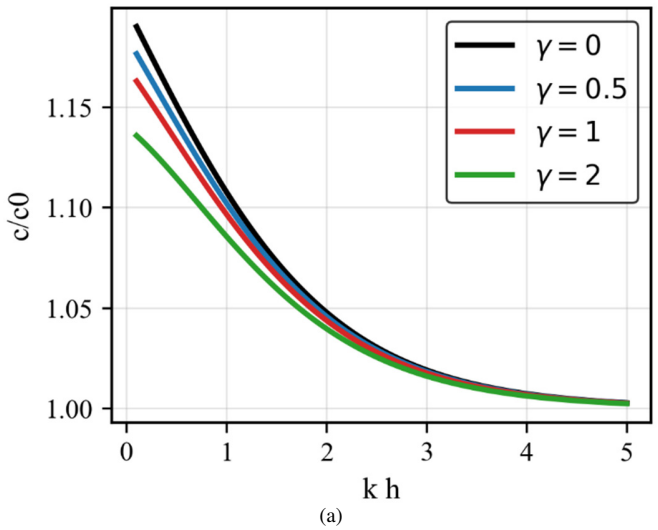

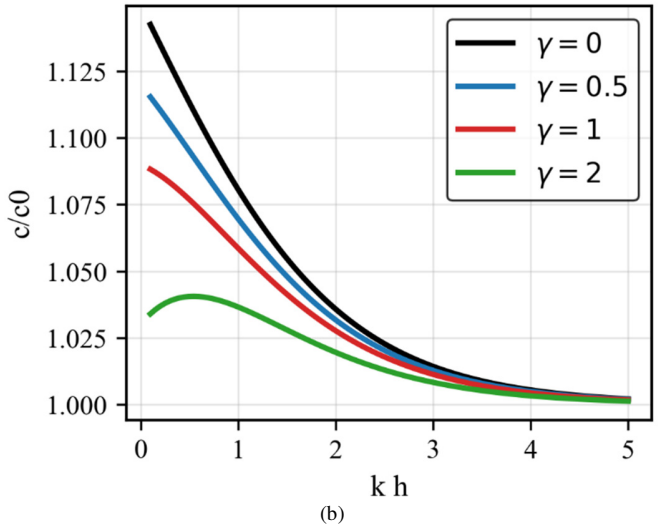

(b)

Fig. 8. Effect of interface parameter R_m on surface wave velocity at a dielectric highly conductive interface (Type 2): (a) open circuit, (b) short circuit.

Figure 9 presents the results for Type 2 (highly conducting) interface. A key observation is that for this interface type, under short-circuit conditions at the surface, the wave velocity becomes virtually independent of the mechanical compliance R_m. This is a significant result, indicating that electrical shorting at the surface can mask the effects of certain interfacial mechanical imperfections.

C. Model Validation

To validate the proposed formulation and numerical scheme, the computed dispersion curves are compared with benchmark results reported in the literature for a homogeneous elastic half-space coated with a homogeneous layer and joined by a perfectly bonded interface. This configuration provides a standard reference case for assessing the accuracy of surface-wave dispersion predictions.

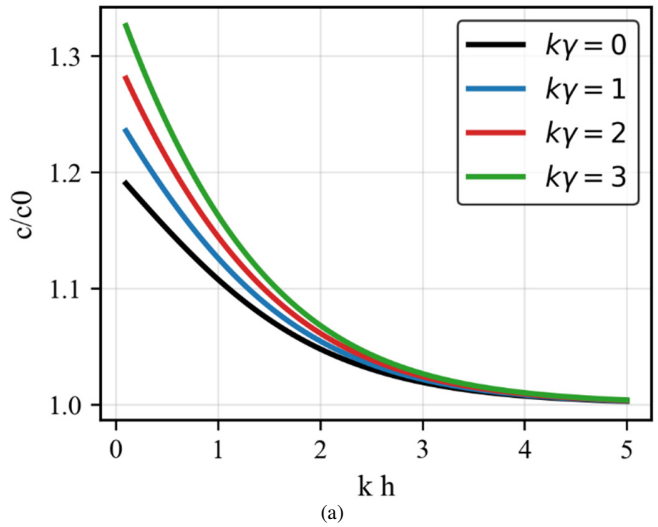

(a)

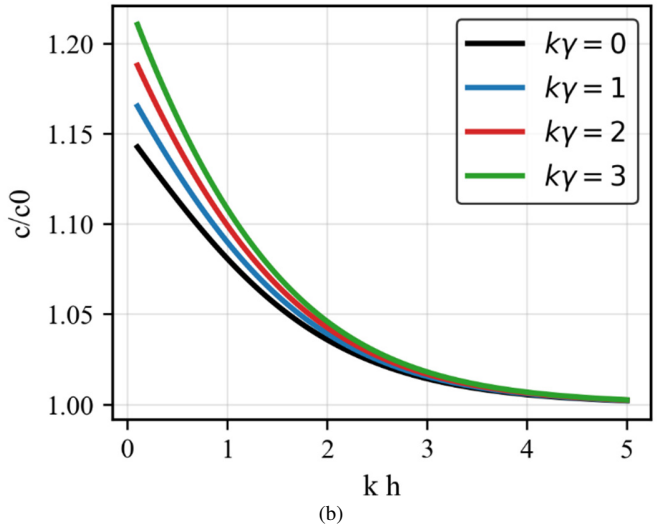

(b)

Fig. 9. Effect of interface parameter $k\gamma$ on surface wave velocity at a dielectric-highly conductive interface: (a) open circuit, (b) short circuit.

Figure 10 shows a direct comparison between the present predictions and those presented in [10] under electrically open-circuit boundary conditions. The two solutions exhibit excellent agreement across the investigated frequency range. Small discrepancies observed at higher frequencies (within 5%) are plausibly attributable to differences in numerical implementation—specifically, the high-order Magnus–Padé strategy adopted here versus discretization-based approaches used in [10]. Overall, this benchmark comparison supports the accuracy and numerical robustness of the proposed model.

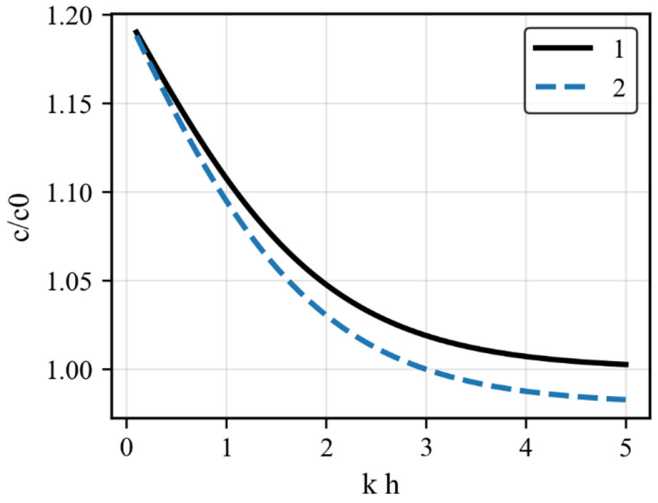

Fig. 10. Comparison of surface-wave phase velocity for a homogeneous elastic half-space with a homogeneous covering layer, coupled via a perfectly bonded interface, under electrically open-circuit boundary conditions. Curve 1 shows the results of the present study, whereas curve 2 reproduces the reference solution from [10].

IV. CONCLUSIONS

A unified analytical–numerical framework is proposed for Rayleigh-wave propagation in an anisotropic elastic half-space

with a functionally graded piezoelectric coating and mechanically/dielectrically non-ideal interfacial conditions. The problem is formulated in state-space form via a transfer-matrix representation and computed using a high-order Magnus–Padé strategy, providing an accurate representation of continuous through-thickness material grading.

This study advances Surface Acoustic Wave (SAW) dispersion modeling by integrating, within a single coherent framework, continuous through-thickness material grading, mechanically/dielectrically imperfect interfacial conditions, and anisotropic substrate behavior. Whereas prior investigations commonly consider these factors separately or represent graded layers through discretized laminates, the present approach accounts for their mutual coupling in a consistent and efficient computational setting.

The present work is distinguished by the use of a high-order Magnus expansion supplemented by Padé approximation to solve the state transfer equation for continuously graded piezoelectric layers with mechanically and/or dielectrically non-ideal interfacial conditions. This treatment circumvents the need for laminate-type discretization of the grading and thereby improves numerical robustness while maintaining accuracy, enabling extensive parametric exploration. The analysis further provides the following physical insights:

1. Rayleigh-wave dispersion can be tailored effectively by the through-thickness gradient profile of the capping layer, producing non-monotonic and frequency-dependent variations in phase velocity that are absent in homogeneous coatings.
2. The sensitivity of the phase velocity to both material grading and interfacial non-idealities is markedly amplified under electrically short-circuit surface conditions.
3. Under short-circuit conditions, a dielectrically highly conducting interface can effectively attenuate (or suppress) the influence of mechanical interfacial compliance on the Rayleigh-wave phase velocity; to the best of our knowledge, this specific coupling effect has not been reported previously.

The contribution of this work to the existing literature is threefold. First, it provides a rigorous quantitative assessment of the effects of through-thickness gradient profiles and interfacial parameters on Rayleigh-wave propagation over low- to medium-frequency regimes. Second, supported by benchmark validation, it demonstrates that functional grading constitutes an effective mechanism for controlling dispersion in piezoelectric surface-wave devices. Third, it offers physically interpretable design guidance that delineates regimes in which interfacial non-idealities must be modeled explicitly from those in which their impact can be reduced through appropriate electrical boundary conditions.

From an applied perspective, the results indicate that realistic modeling of SAW devices necessitates the concurrent consideration of fabrication-induced material grading and interfacial degradation effects. In this regard, the proposed framework provides a reliable theoretical tool for both the design and non-destructive evaluation of advanced SAW-based sensors, filters, and microsystems.

Future work may extend the present formulation to viscoelastic and thermo-electro-mechanical material models, more general interfacial constitutive descriptions, and additional guided-wave modes, such as Love waves or plate waves, in functionally graded piezoelectric structures.

ACKNOWLEDGMENT

The authors acknowledge with gratitude the institutional support of Karshi State University and appreciate the valuable discussions and technical assistance provided by their colleagues.

REFERENCES

[1] S. V. Biryukov, Y. V. Gulyaev, V. V. Krylov, and V. P. Plessky, *Surface Acoustic Waves in Inhomogeneous Media*, 1st ed. Berlin, Heidelberg, Germany: Springer, 1995, https://doi.org/10.1007/978-3-642-57767-3.

[2] D. Morgan, *Surface Acoustic Wave Filters: With Applications to Electronic Communications and Signal Processing*, 2nd ed. San Diego, CA, USA: Academic Press, 2007, https://doi.org/10.1016/B978-0-12-372537-0.X5000-6.

[3] K. Hashimoto, *Surface Acoustic Wave Devices in Telecommunications*. Berlin, Heidelberg, Germany: Springer, 2000, https://doi.org/10.1007/978-3-662-04223-6.

[4] J. D. Achenbach, *Wave propagation in elastic solids*. Amsterdam, Netherlands: North-Holland Publishing Co., 1973.

[5] S. Chiriță, "Thermoelastic surface waves on an exponentially graded half-space," *Mechanics Research Communications*, vol. 49, pp. 27–35, Apr. 2013, https://doi.org/10.1016/j.mechrescom.2013.01.005.

[6] X. Cao, F. Jin, and I. Jeon, "Rayleigh surface wave in a piezoelectric wafer with subsurface damage," *Applied Physics Letters*, vol. 95, no. 26, Dec. 2009, Art. no. 261906, https://doi.org/10.1063/1.3276568.

[7] X. Wang and L. J. Sudak, "A piezoelectric screw dislocation interacting with an imperfect piezoelectric bimaterial interface," *International Journal of Solids and Structures*, vol. 44, no. 10, pp. 3344–3358, May 2007, https://doi.org/10.1016/j.ijsolstr.2006.09.022.

[8] I. Ben Salah, A. Njeh, and M. H. Ben Ghozlen, "A theoretical study of the propagation of Rayleigh waves in a functionally graded piezoelectric material (FGPM)," *Ultrasonics*, vol. 52, no. 2, pp. 306–314, Feb. 2012, https://doi.org/10.1016/j.ultras.2011.08.016.

[9] M. M. Charshamievich, "Stability and Accuracy of the Hybrid Method for Dynamic Half- Space Models under Sinusoidal Impulsive Surface Loads," (in Russian) *International Journal of Science*, vol. 2, no. 1, pp. 15–20, Apr. 2025.

[10] M. Matanov, "Harmonic Fundamental Solutions and Boundary Integral Equations for Wave Propagation in Elastic, Scalar and Poroelastic Media," *ACTA NUUz*, vol. 2, no. 2.1.1, pp. 80–87, Nov. 2025.

[11] V. N. Dorovsky, *Equations of the continual theory of filtration*. Novosibirsk, Russia: IGiG SB USSR Academy of Sciences (in Russian), 1987.

[12] H. Chang, F. Wang, X. Yue, L. Qiu, and L. Sun, "A 2.5D Generalized Finite Difference Method for Elastic Wave Propagation Problems," *Mathematics*, vol. 13, no. 8, Apr. 2025, Art. no. 1249, https://doi.org/10.3390/math13081249.

[13] A. Mallick and S. Biswas, "Thermoelastic diffusion in nonlocal orthotropic medium with porosity," *Composite Structures*, vol. 337, June 2024, Art. no. 118043, https://doi.org/10.1016/j.compstruct.2024.118043.

[14] A. Mallick and S. Biswas, "Rayleigh waves in nonlocal orthotropic thermoelastic medium with diffusion," *Heat Transfer*, vol. 54, no. 1, pp. 271–306, Jan. 2025, https://doi.org/10.1002/htj.23169.

[15] I. M. Khalatnikov, *Theory of Superfluidity*. Moscow, Russia: Nauka (in Russian), 1971.

[16] S. Blanes, F. Casas, J. A. Oteo, and J. Ros, "The Magnus expansion and some of its applications," *Physics Reports*, vol. 470, no. 5, pp. 151–238, Jan. 2009, https://doi.org/10.1016/j.physrep.2008.11.001.

[17] A. Xolmurodov, M. Matanov, and M. Quzratov, "Propagation of harmonic plane waves in an elastic half-space. Field equations," *AIP Conference Proceedings*, vol. 3244, no. 1, Nov. 2024, Art. no. 020019, https://doi.org/10.1063/5.0241519.

[18] A. E. Kholmurodov and M. C. Matanov, "Seismic excitation model of half-space propagation of rayleigh waves," (in Russian) *Problems of Computational and Applied Mathematics*, no. 6(62), pp. 45–56, 2024.

[19] T. Nagao and X. Ma, "The Impact of Ground Irregular Sedimentary Structure on the Seismic Motion Amplification Characteristics: A case study in Tottori, Japan," *Engineering, Technology & Applied Science Research*, vol. 13, no. 3, pp. 10834–10842, June 2023, https://doi.org/10.48084/etasr.5785.

[20] M. S. Vijaya, *Piezoelectric Materials and Devices: Applications in Engineering and Medical Sciences*, 1st ed. Boca Raton, FL, USA: CRC Press, 2013, https://doi.org/10.1201/b12709.